Power Electronic Systems
Laboratory

IEEE/ASME Transactions on Mechatronics, Vol. 20, Issue 1, pp. 37-49, February 2015

High-Temperature (250 °C / 500 °F) 19 000 min-1 BLDC Fan for Forced Air-Cooling of Advanced Automotive Power Electronics

B. Wrzecionko,
J. W. Kolar,
A. Looser,
M. Casey

Eidgenössische Technische Hochschule Zürich
Swiss Federal Institute of Technology Zurich

High-Temperature (250 °C / 500 °F) 19 000 min^{-1} BLDC Fan for Forced Air-Cooling of Advanced Automotive Power Electronics

Benjamin Wrzecionko, *Student Member, IEEE*, Andreas Looser, *Student Member, IEEE*, Johann W. Kolar, *Fellow, IEEE*, and Michael Casey

***Abstract*—In an increasing number of application areas and industry sectors, such as the automotive, aerospace, military, or oil and gas industry, a trend towards higher ambient temperature rating from 120 °C upward for electrical machines and power electronic converters can be observed. Forced air-cooling of power electronic converters offers reduced complexity of the cooling circuit compared to water-cooling. For air-cooled, high-ambient temperature rated converters, fans are required to withstand these temperatures and still feature performance comparable to standard conditions in order to still enable a high converter power density and efficiency. Commercially available fans for power electronics cooling are typically rated up to 75 °C, rarely fans are specified up to 105 °C. In this paper, the electrical and mechanical design of a 40 mm × 40 mm × 28 mm fan is presented in detail that offers an operational temperature range from −40 °C to 250 °C at the rated speed of 19 000 min^{-1} and comparable fluid dynamic performance in terms of static pressure and volume flow at 120 °C as commercial high performance fans at 20 °C. The three-phase brushless direct current machine driving the fan is integrated into its hub and has got an input power of 15 W. The fan can be driven using a three-phase inverter supplied from 12 V dc voltage with an inverter switching frequency of less than 1.3 kHz.**

***Index Terms*—Automotive components, brushless machines, fans, high-temperature techniques, permanent-magnet machines.**

I. Introduction

AUTOMOTIVE power electronic converters have substantially gained research and development interest triggered by the increasing market share of hybrid electric vehicles (HEVs) [1]. Compared to conventional drive concepts, where the vehicle is driven by an internal combustion engine (ICE) only and power electronic converters are solely found in auxiliary drives or power supplies, typically a series-connections of dc–dc and dc–ac converter(s) is used to drive the electrical machine(s) in the drive train of the HEV. Hence, the power level of automotive power electronic converters is currently increasing by orders of magnitude; the power level of a conventional alternator and its rectifier is below 5 kW for a passenger car [2], while the power level of the electrical machine can be as high as 160 kW as for the 2008 Lexus model "LS 600h" [3].

The power electronic converters, especially the dc–ac drive inverters, are placed underneath the engine hood in the majority of today's HEVs, close to the electrical machine in order to transmit the high voltages of the inverter switched at high frequencies over short distances only. The electrical machine is mechanically coupled to drive train components such as the ICE and the gearbox and is positioned in close vicinity to them. The ambient temperature in the engine compartment can reach 120 °C (and even higher values around 650 °C close to the exhaust system) [4]–[6]. Today's automotive power electronic converters employ silicon (Si) power semiconductors with an upper junction temperature limit between 150 °C and 175 °C. In order to establish a sufficiently large temperature difference between the Si power semiconductor junction and the ambience, the "ambient" temperature of the converter is artificially lowered by water-cooling using a water–glycol mixture with a maximum temperature around 50 °C to 70 °C, that is separated from the cooling circuit of the ICE [7], [8].

Using the wide bandgap power semiconductor silicon carbide (SiC) as well as novel joining and bonding technologies such as sintered silver die attachment and copper bonding, the junction temperature of the power semiconductors can be increased to values higher than 175 °C [9]–[13]. This allows to establish a sufficiently high temperature difference between the power semiconductor junction and the ambient temperature level, even if the ambient temperature of the converter is raised to 120 °C by using the water–glycol cooling circuit of the ICE or by direct air-cooling using the ambient air underneath the engine hood [14]–[16]. With respect to cost and complexity of the cooling system, direct air-cooling can represent a superior solution as no pumps, water pipes, and water–air heat exchangers are needed. A junction temperature around 250 °C for typical SiC power semiconductors at 120 °C ambient temperature has been calculated to be close to the optimum junction temperature with respect to chip utilization and power density for an 120 °C ambient-air-cooled dc–ac inverter [17], [18].

With direct air-cooling of automotive power electronic converters at 120 °C ambient and 250 °C junction temperature, not

Manuscript received June 3, 2013; revised August 27, 2013 and November 5, 2013; accepted December 20, 2013. Date of publication March 25, 2014; date of current version October 3, 2014. Recommended by Technical Editor K.-S. Hwang.

B. Wrzecionko and A. Looser were with the Power Electronic Systems Laboratory, Swiss Federal Institute of Technology Zurich (ETH Zurich), 8092 Zurich, Switzerland (e-mail: wrzecionko@lem.ee.ethz.ch; looser@lem.ee.ethz.ch).

J. W. Kolar is with the Power Electronic Systems Laboratory, Swiss Federal Institute of Technology Zurich (ETH Zurich), 8092 Zurich, Switzerland (e-mail: kolar@lem.ee.ethz.ch).

M. Casey, retired, was with the Institute of Thermal Turbomachinery and Machinery Laboratory, University of Stuttgart, 70550 Stuttgart, Germany (e-mail: casey@itsm.uni-stuttgart.de).

Color versions of one or more of the figures in this paper are available online at http://ieeexplore.ieee.org.

Digital Object Identifier 10.1109/TMECH.2014.2309481

only the power semiconductors and their packaging, but also the signal electronics, the passive components like dc-link capacitors as well as the components of the air-cooling system such as thermal interface materials, heat sinks, and fans need to withstand these harsh temperature conditions. For the signal electronics and passives, a converter setup dealing with the challenges induced by 120 °C ambient and 250 °C junction temperature has been presented with Si signal electronics actively cooled by a Peltier cooler in order to make sure their operating temperature limit of 125 °C is maintained [15]. Thermally conductive interface materials are available up to 300 °C [19], heat sinks are typically made of aluminum or copper and, thus, withstand these temperatures as well.

With respect to the high temperature capability of available fans, the picture changes significantly: Most of the commercially available dc fans suitable for designing compact power electronic converters, i.e., those having a high pressurization and volume flow with respect to their volume, suffer from operating temperature limits below or equal 75 °C. The electrical and mechanical design of these fans might allow the manufacturer to test and specify the devices for somewhat higher ambient temperatures with only slight component changes. Still, the lifetime of the ball bearings used in, e.g., Sanyo Denki fans with high performance concerning pressurization and volume flow related to the volume, is cut in half for each 15 K ambient temperature increase and the maximum operating temperature is 105 °C [20].

Other fan manufacturers sell fans for electronics cooling with temperature ratings up to 90 °C but these fans suffer from larger size and lower fluid dynamics performance compared to the Sanyo Denki models [21]. Other solutions available on the market are fans for ovens with recirculating air that are not equipped with an electrical machine in the hub but have it placed externally to reduce the ambient temperature for the electrical machine. The fan is then driven by a belt or a shaft which results in a more bulky setup and available rotational speeds are typically lower.

High ambient temperature electrical machines for integration into the fan hub are currently also investigated for other application areas, especially in the aerospace and downhole industry. Research for expeditions to Venus have yield switched reluctance machines for up to 540 °C, but they are designed for an operational lifetime of only 50 days [22]. Furthermore, deeper oil reservoirs are currently explored, where electrical submersible pumps are used to provide a continuous flow of oil up to the surface [23]. The electrical machines used in such pumps can withstand temperatures up to 218 °C [24].

In this paper, a high temperature brushless direct current (BLDC) machine fan withstanding an ambient temperature of 250 °C with a rotational speed of 19 000 min^{-1} for forced air-cooling of advanced automotive power electronics is presented (see Fig. 1 and Table I). The BLDC electrical machine driving the fan is integrated into the hub of the fan and, thus, can withstand 250 °C ambient temperatures as well. The power electronic inverter for the BLDC machine can be realized on a separate printed-circuit board, that is part of the 120 °C ambient temperature rated dc–ac traction inverter [15], [25], [26].

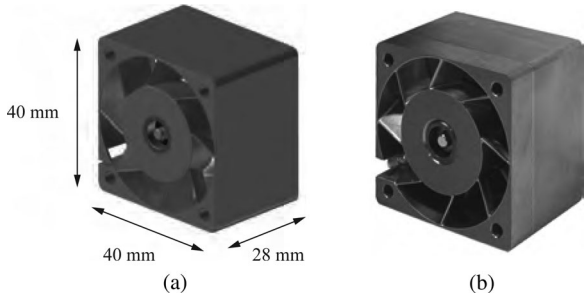

Fig. 1. (a) CAD picture and (b) photograph of high-temperature (250 °C/500 °F) 19 000 min^{-1} BLDC fan for forced air-cooling of advanced automotive power electronics.

TABLE I
OVERVIEW OF HIGH-TEMPERATURE FAN SPECIFICATIONS

High-Temperature Fan	
Air Temperature (maximum) $T_{\max}$	250 °C
Max. Static Pressure (at 20 °C) $\Delta p_{\max,\mathrm{HTF}}$	408 Pa
Max. Volume Flow (at 20 °C) $\dot{V}_{\max,\mathrm{HTF}}$	0.84 m^3/min
Rotational Speed n_{HTF}	19'000 min^{-1}
Electrical Input Power $P_{\mathrm{el,HTF}}$	12 W
Terminal Voltage rms V_{HTF}	8.5 V[1]
Phase Current rms I_{HTF}	0.8 A
Electrical Frequency $f_{\mathrm{el,HTF}}$	1267 Hz
Mass m_{HTF}	96 g
Electrical Machine Type	3ph BLDC

[1]A fan inverter dc input voltage of 12 V is sufficient to drive the fan with rated speed at nominal operating point.

The fluid dynamic performance of the fan in terms of static pressure and volume flow at the nominal ambient temperature of 120 °C for power electronic converters placed under the engine hood in HEVs is comparable to that of commercial high performance fans at their nominal ambient temperature of 20 °C. The 250 °C specification gives designers of high-junction-temperature SiC power electronic converters more degrees of freedom for arranging the converter components as the fans can also be placed on the air outlet side of the heat sink so that they draw the hot air out of the heat sink rather than blowing it into the heat sink. Then, an arrangement with a fan in between two heat sinks is also possible.

It is shown in detail in Section II, how the fan specifications, i.e., the dimensions, fluid dynamic performance, and machine characteristics are derived with respect to the needs induced by air-cooling of ultracompact automotive power electronic converters for high ambient temperatures. Subsequently, the design of the electrical machine and mechanical parts is carried out in Section III and Section IV, respectively. Finally, experimental results in terms of electrical voltage, current, and power as well as fluid dynamic and acoustical measurements are presented in Section V.

II. FAN SPECIFICATIONS

A. Air-Cooling of Power Electronics

In general, the cooling system of a power electronic converter has to dissipate the power loss of components within the

converter via a thermally conductive path to the ambience, where a thermal resistance R_{th} should be as low as possible. At the same time, the cooling system is required to have a volume V_{CS} as small as possible in order to facilitate a high power density of the converter, leading to the definition of the *cooling system performance index* which is the inverse of the product of R_{th} and V_{CS} [27].

To make sure that the thermal resistance $R_{\mathrm{th,HA}}$ of the heat sink does not increase significantly throughout the operation of the power electronic converter due to dust congesting the heat sink air channels, an air filtering system has to be deployed. This filtering system should clean the air before it is blown through the heat sinks by the fans and can be similar to what is already well known in the automotive industry for use with ICEs. Accordingly, considerations regarding ingress protection rating affect more the overall design of the complete power electronic converter system than the fans.

Furthermore, standard requirements for technical systems apply also for power electronic cooling systems: low system complexity, low manufacturing and maintenance cost, low size, low weight, low power consumption, low noise generation, and low performance invariance against deterioration or spread for standard factory models.

B. Air Flow Direction

The applicability of a certain fan for a forced air-cooling setup within a power electronic converter can be assessed based on the direction of the air flow it produces: centrifugal or radial fans can hardly be integrated into a typical setup without modifications where lossy components, e.g., power semiconductors, are mounted on heat sinks with extruded fins. A modified centrifugal fan, that guides the radial air flow into a tangential direction, is called a blower. These fans deliver high pressure and volume flow for a certain outlet cross-section of the fan compared to axial fans, but their overall volume is usually significantly larger.

The most common fans with the largest variety of models for power electronics cooling are diagonal and axial flow fans. The difference between both fans is that for diagonal fans the housing and sometimes also the blades are conical with a larger diameter at the fan outlet, so that the air is guided not only in axial direction out of the fan but also shows a small radial velocity component. This allows the fan to produce higher pressure at a higher volume flow for the same size and power rating. It has to be mentioned though, that it is strongly dependent on the geometry of the heat sink attached to the fan outlet and the attachment itself (e.g., spacing between fan outlet and heat sink) whether the diagonal component of the air flow is utilized or whether the air is directed back into the axial direction by the heat sink. In fact, most fans that are referred to as "axial" are constructed as slightly diagonal fans. Hence, in this paper, the terminology will be the same as usual and these fans will be referred to as axial. Some of the axial fans have guide vanes at the outlet side of the housing to reduce the air spin produced by the rotating vanes.

Counter rotating axial fans are equipped with two rotors that rotate in opposite directions yielding a high pressurization. Optimizing the fin design of the heat sink for the use with such fans with respect to the thermal resistance of the heat sink leads to very thin fins with very small spacing in between them which makes the manufacturing process very expensive and is only available for small aspect ratios of fin height to fin thickness [27]. Therefore, the additional pressure does usually not pay off in terms of power density.

Hence, the high temperature fan in this paper is designed as a single stage axial flow fan with guide vanes.

C. Physical Dimensions

The length of the outlet cross-section edges of the high temperature fan is set with regard to ubiquitous applicability as 40 mm $\times$ 40 mm [see Fig. 1(a)]. This corresponds to the largest fans that are commercially available while still being below the size of one rack unit, which is 1 U $= 1.75$ in $= 44.45$ mm. For reference purposes and the sake of compatibility, the axial length of the high temperature fan is chosen to 28 mm which equals the length of the Sanyo Denki model "San Ace 40 GV" [28] with best-in-class static pressure over volume flow characteristics.

D. Static Pressure Versus Volume Flow at Increased Ambient Temperatures

The fluid dynamic characteristic of a fan as well as the heat sink fin and baseplate design determine the resulting thermal resistance $R_{\mathrm{th,HA}}$ from the heat sink surface (which carries the lossy components) to the ambience (to which the heat is dissipated). The fluid dynamic characteristic is usually given as a difference in static pressure Δp between the outlet and inlet side of the fan versus its volume flow $\dot{V}$ for a certain rotational speed n of the fan rotor.

This characteristic curve depends largely on the measurement conditions especially with respect to the air density ρ, which is mainly given by air temperature T and absolute air pressure p. Fan manufacturers often measure the curve according to the standard "AMCA 210-85", set by the Air Movement and Control Association (AMCA) International [29], [30]. The reference air temperature is set to $T_{\mathrm{ref}} = 20\,^{\circ}\mathrm{C}$ and the absolute hydrostatic pressure of the air to $p = 1.013 \cdot 10^{5}\mathrm{Pa}$ [29].

In Fig. 2,the curve of the commercial high performance fan Sanyo Denki San Ace 40 GV for a rotational speed of $n_{\mathrm{RF}} = 16'500\,\mathrm{min}^{-1}$ [28] is given as an example. Also shown in this figure is the parabolic characteristic of the heat sink, i.e., the fluid dynamic load characteristic, which divides the characteristic curve of the fan into two parts: the right part starts at free air conditions with maximum volume flow $\dot{V} = \dot{V}_{\mathrm{max}}$ and shows a linear correlation between $\dot{V}$ and Δp. The intersection point of curve and parabola is advantageously selected in the region where the gradient of the curve changes and approaches zero and goes even positive, i.e., where Δp decreases (slightly) with decreasing $\dot{V}$. This happens for the Sanyo Denki San Ace 40 GV for $\dot{V}_{\mathrm{S}} = 0.56\,\mathrm{m}^3/\mathrm{min}$. In this region, airflow separation at the fan blades occurs and the fan stalls leading to a significantly affected air-side performance as well as noisy and surging air

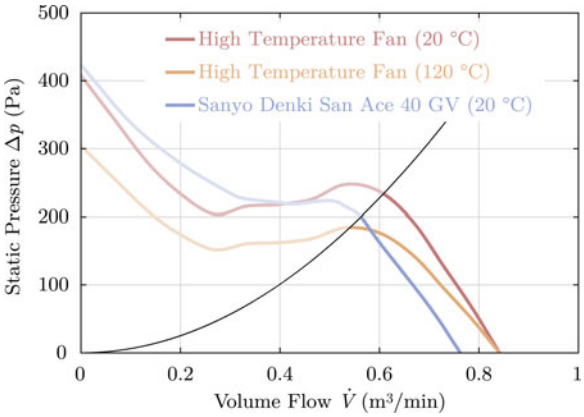

Fig. 2. Static pressure over volume flow curves for the high temperature fan presented in this paper with 19 000 min^{-1} at 20 °C and 120 °C as well as for the Sanyo Denki reference fan with 16′500 min^{-1}. The fluid dynamic design criteria for the high temperature fan at 120 °C in terms of $\dot{V}_{\max}$ and Δp is fulfilled for the largest part of the characteristic curve given by the parabola of operation.

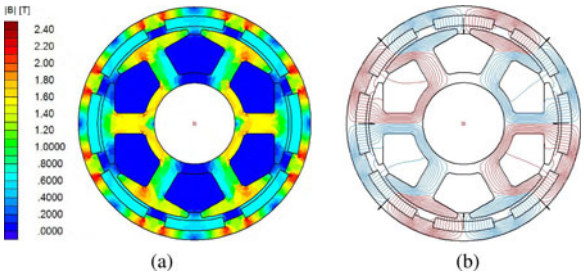

Fig. 3. (a) Flux density distribution under full load condition. The flux density in the stator and yoke is less than 2.1 T which is below the saturation limit of 2.35 T of the employed iron cobalt material (see Section III-B and Section III-D). (b) Magnetic field lines under no load condition of the BLDC machine.

flow. For smaller volume flows, the blades move the air by centrifugal forces until zero air flow $\dot{V} = 0$. For a safe, reliable, and efficient operation of the fan, the fluid dynamic load (e.g., a heat sink) has to be chosen such that the intersection of the load line and the fan curve are in the right part of the fan curve [29]. As mentioned in Section I, the design target is to have an equal or better fluid dynamic characteristic within the relevant part of the characteristic curve at the nominal operating air temperature, i.e., at $T_{\text{nom}} = 120\,^{\circ}\text{C}$, than that of the San Ace 40 GV reference fan at $T_{\text{ref}} = 20\,^{\circ}\text{C}$.

To analyze the impact of increased ambient temperature on the performance of a fan, first, the correlation between air density ρ and air temperature T is found using the ideal gas law (1). It is valid for vanishing absolute pressures $p \to 0$, but for almost all real gases, including dry air, deviations from the ideal behavior are negligible at atmospheric pressures [31]. The temperature independent gas constant is $R = 287.05\,\frac{\text{J}}{\text{kg}\cdot\text{K}}$ for dry air and the absolute pressure is with $p = 101.325\,\text{kPa}$ [32] the same as for standard conditions because the air underneath the engine hood in HEVs can expand when heated by the ICE, and hence, this change of state is of isobar type [33],

$$\rho = \frac{p}{R \cdot T} = \begin{cases} 1.20 & \text{for} \quad T = 20\,^{\circ}\text{C} \\ 0.90 \quad \text{kg/m}^3 & \text{for} \quad T = 120\,^{\circ}\text{C}. \\ 0.67 & \text{for} \quad T = 250\,^{\circ}\text{C} \end{cases} \tag{1}$$

The high-temperature fan will be operated in speed controlled mode; hence, the rotor speed n is constant within the operating temperature range of the fan. Even with varying air density, this leads to a constant volume flow $\dot{V}$ of the fan [34]

$$\dot{V} = \text{const} \quad \text{for} \quad n = \text{const}. \tag{2}$$

However, $\Delta p(T)$ and the mechanical shaft power $P_{\text{S}}(T)$ of the fan scale proportionally with ρ leading to an inversely proportional correlation with T for $n = \text{const}$ [34],

$$\frac{\Delta p(T)}{\Delta p(T_{\text{ref}})} = \frac{P_{\text{S}}(T)}{P_{\text{S}}(T_{\text{ref}})} = \frac{T_{\text{ref}}}{T} = \begin{cases} 1 & \text{for} \quad T = 20\,^{\circ}\text{C} \\ 0.75 & \text{for} \quad T = 120\,^{\circ}\text{C}. \\ 0.56 & \text{for} \quad T = 250\,^{\circ}\text{C} \end{cases} \tag{3}$$

The impact on the characteristic curve of the fan can be seen in Fig. 2, where the fluid dynamic characteristic of the high temperature fan is shown for $T_{\text{ref}} = 20\,^{\circ}\text{C}$ and $T_{\text{nom}} = 120\,^{\circ}\text{C}$. With respect to the change in power, it has to be noted, that the input power P_{el} of a fan may not decrease by the same amount as the mechanical shaft power does due to decreasing fan motor and inverter efficiency at higher temperatures.

The reduction in static pressure from the reference fan at $T_{\text{ref}} = 20\,^{\circ}\text{C}$ to the high temperature at $T_{\text{nom}} = 120\,^{\circ}\text{C}$ caused by an increased temperature can be compensated by increasing the rotor speed of the fan from n_{RF} of the San Ace 40 GV fan to n_{HTF} for the high temperature fan.

To derive the exact correlation between n_{RF} and n_{HTF}, the following fan scaling laws can be used for $T = \text{const}$ [27],

$$\dot{V} = k_1 \cdot n \cdot d^3 \tag{4}$$

$$\Delta p = k_2 \cdot n^2 \cdot d^2 \tag{5}$$

$$P_{\text{el}} = k_3 \cdot n^3 \cdot d^5. \tag{6}$$

The diameter of the fan rotor is denoted by d (which is often approximated by the edge length of the quadratic outlet or inlet cross-section), the electrical input power by P_{el} and $k_i, i = \{1, 2, 3\}$, represent factors of proportionality depending on the design of a specific fan. k_1 and k_2 vary only by a factor of two from one fan to another for most commercial fans [27]. Assuming a similar fluid dynamic design of the reference fan and the high temperature fan in terms of the fan dimensions as well as the rotor and stator guide vanes, k_1 and k_2, respectively, will be very similar for the two fans. In order to meet the fluid dynamic design target of the high temperature fan, the following constraint has to be fulfilled for volume flows $\dot{V}_{\text{S}} = 0.56\ \text{m}^3/\text{min} \leq \dot{V} \leq \dot{V}_{\max}$:

$$\Delta p_{\text{HTF}}(T_{\text{nom}} = 120\,^{\circ}\text{C}) \overset{!}{\geq} \Delta p_{\text{RF}}(T_{\text{ref}} = 20\,^{\circ}\text{C}). \tag{7}$$

It can be seen from (3) that $\Delta p_{\max,\text{HTF}}(T_{\text{ref}})$ of the new high temperature fan has to be higher by a factor of $T_{\text{nom}}/T_{\text{ref}}$ than

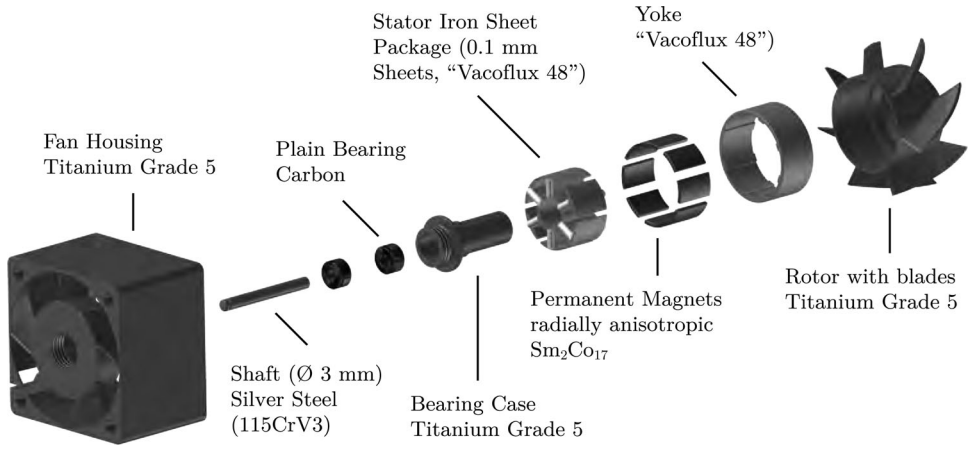

Fig. 4. Exploded view drawing of high-temperature (250 °C/500 °F) 19 000 min^{-1} BLDC fan for forced air-cooling of advanced automotive power electronics.

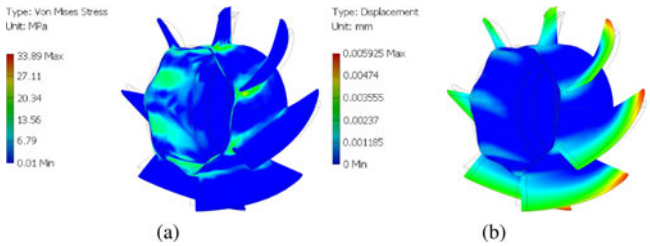

Fig. 5. FEM simulation of rotor (a) von Mises stress and (b) displacement at a rotational speed of 19 000 min^{-1} and an ambient temperature of 300 °C. A safety margin of more than 15 for the maximum stress is included for the designed Titanium Grade 5 rotor.

the pressure $\Delta p_{\mathrm{max,RF}}(T_{\mathrm{ref}})$ of the reference fan in order to meet (7). With (5), n_{HTF} can be calculated as

$$n_{\mathrm{HTF}} = n_{\mathrm{RF}} \sqrt{\frac{\Delta p_{\mathrm{max,HTF}}(T_{\mathrm{ref}})}{\Delta p_{\mathrm{max,RF}}(T_{\mathrm{ref}})}} = n_{\mathrm{RF}} \sqrt{\frac{T_{\mathrm{nom}}}{T_{\mathrm{ref}}}}$$

$$= 16'500\,\mathrm{min}^{-1} \cdot \sqrt{\frac{393.15\,\mathrm{K}}{293.15\,\mathrm{K}}} \approx 19\,000\,\mathrm{min}^{-1}. \quad (8)$$

According to (4), the increased speed n_{HTF} also leads to an increase in volume flow of the high temperature fan. The maximum volume flow $\dot{V}_{\mathrm{max,HTF}}$ can be calculated compared to the maximum volume flow $\dot{V}_{\mathrm{max,RF}}$ of the reference fan as

$$\dot{V}_{\mathrm{max,HTF}} = \frac{n_{\mathrm{HTF}}}{n_{\mathrm{RF}}} \cdot \dot{V}_{\mathrm{max,RF}} = 0.88\ \mathrm{m}^3/\mathrm{min}. \quad (9)$$

Furthermore, the shaft power P_{S} is also increased for the high temperature fan as it scales with n^3 [34]. The rise in shaft power for the nominal operating point T_{nom} of the high temperature fan compared to the nominal operating point T_{ref} of the reference fan is not as high as expected from the cubic correlation as the temperature rise from T_{ref} to T_{nom} reduces the required shaft power according to (3). The exact increase in shaft power $P_{\mathrm{S,HTF}}$ for the high temperature fan can be derived as

$$P_{\mathrm{S,HTF}}(T) = P_{\mathrm{S,RF}}(T) \cdot \left(\frac{n_{\mathrm{HTF}}}{n_{\mathrm{RF}}}\right)^3$$

$$= P_{\mathrm{S,RF}}(T_{\mathrm{ref}}) \cdot \sqrt{\frac{T_{\mathrm{nom}}^3}{T_{\mathrm{ref}}}} \cdot \frac{1}{T}$$

$$= P_{\mathrm{S,RF}}(T_{\mathrm{ref}}) \begin{cases} 1.55 & \text{for} \quad T = 20\,^{\circ}\mathrm{C} \\ 1.16 & \text{for} \quad T = 120\,^{\circ}\mathrm{C}. \\ 0.87 & \text{for} \quad T = 250\,^{\circ}\mathrm{C} \end{cases} \quad (10)$$

The shaft power $P_{\mathrm{S,RF}}(T_{\mathrm{ref}})$ of the reference fan and, thus, the output power of its electrical machine is unknown; the electrical input power $P_{\mathrm{el,RF}}$ is 10.1 W at T_{ref} [28]. If a similar efficiency of the electrical machine for both fans is assumed, the required input power $P_{\mathrm{el,HTF}}$ of the high temperature fan can be specified to 15 W. This makes the operation of the high temperature fan at rated speed n_{HTF} even at $T_{\mathrm{ref}} = 20\,^{\circ}\mathrm{C}$, i.e., 100 K below its nominal operating point $T_{\mathrm{nom}} = 120\,^{\circ}\mathrm{C}$, possible.

The results of this section will be validated along with other experimental data in Section V.

E. Electrical Machine

1) General: In order to achieve a compact fan design (see Section II-A), the electrical machine has to be integrated into the hub of the high temperature fan. Hence, the machine must be able to withstand an ambient temperature of 250 °C plus the self-heating due to its losses. Typically, an internal fan motor is designed as a machine with an external rotor as this simplifies the mechanical construction and the usual drawbacks of external rotor machines such as higher rotational mass with a larger distance to the axis of rotation, both of which lead to a higher moment of inertia than for an internal rotor machine, are of less importance for fan operation where the moment of inertia smoothes a potential cogging torque and the speed control is not required to be highly dynamic.

The input power of the machine is determined in Section II-D to 15 W at its nominal operating point with a rated speed of 19 000 min^{-1}. As this fan is designed for cooling of automotive power electronics, the machine should be able to be driven by an inverter supplied from a 12 V dc bus.

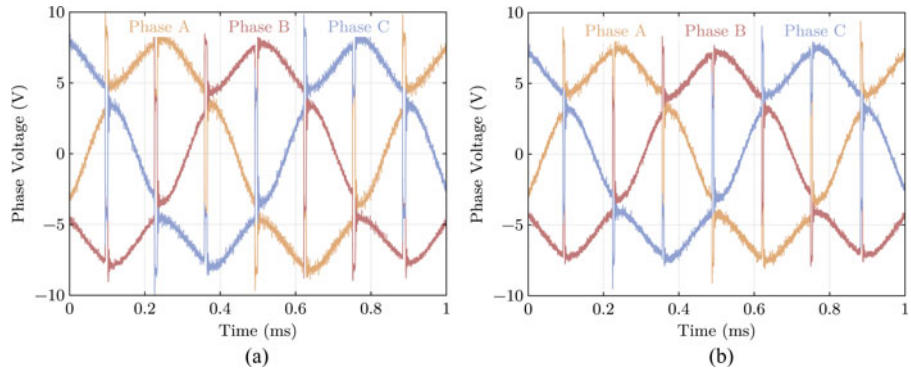

Fig. 6. Three-phase voltages of the high temperature fan at ambient temperatures of (a) 25 °C and (b) 250 °C under closed loop speed control. The rotational speed is 19 000 min^{-1}.

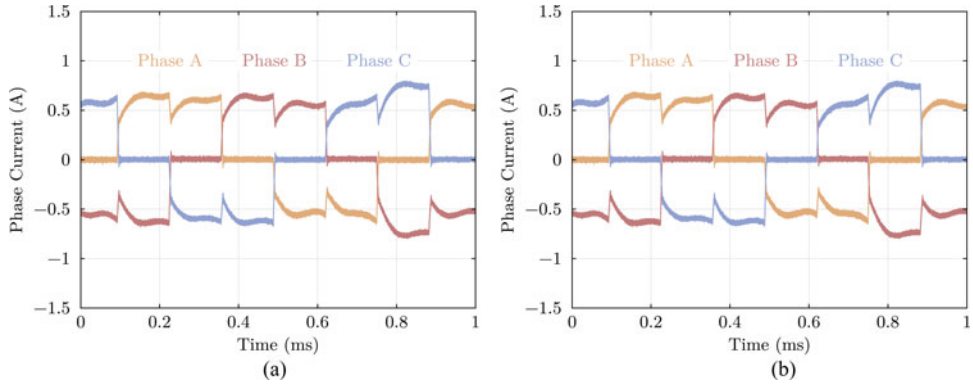

Fig. 7. Three-phase currents of the high temperature fan at ambient temperatures of (a) 25 °C and (b) 250 °C under closed loop speed control. The rotational speed is 19 000 min^{-1}.

2) Machine Type: Possible types of electrical machines can be based on either electric or magnetic fields. With respect to the machine dimensions with an outer diameter of 23 mm and an axial length of 10 mm (restricted by the mechanical design, see Section IV), those using magnetic fields for the electromechanical energy conversion are preferable due to a higher energy and force density [35], [36]. Possible concepts are induction, permanent magnet, switched reluctance, or conventional dc machines with brushes or brushless dc machines. At first sight, induction and switched reluctance machines appear as favorable choices for harsh environmental conditions as they are regarded as very robust machines without need for expensive and temperature sensitive permanent magnets.

Still, it has to be considered, that the motor torque is generated by the stator and rotor flux components which can both be electromagnetically excited; alternatively, one set of windings could be replaced by permanent magnets. The flux density caused by a permanent magnet is constant for varying machine dimensions while the rated current of an electrical machine decreases with decreasing machine dimensions. Hence, for small drives with diameters of less than 100 mm like given in this case, machines with permanent magnets, i.e., dc or synchronous machines, are the favorable choice if a high power density is needed [36], [37].

Conventional dc machines with brushes can be driven from a constant dc voltage source in their nominal operating point so that no additional inverter is necessary which is advantageous especially at such harsh environmental conditions. Still, the brushes suffer from significant wear and affect the reliability. If the fan is required to be speed controlled in order to make sure that the fluid dynamic performance varies only little over the complete temperature range of approximately 300 K, additional controls are needed. Furthermore, a dc machine with brushes designed as with an external rotor requires additional mechanical effort.

Hence, the integrated machine of the high temperature fan will be designed as a BLDC machine which is constructed as permanent-magnet synchronous machines (the magnetic design can be slightly different to make the rotor produce a rectangular rather than a sinusoidal back electromotive force) but is driven with (in case of a three-phase machine) 120° phase-shifted rectangular voltages instead of pulse-width modulated voltages which would allow to achieve a sinusoidal current waveform. This gives a slightly higher torque and allows to reduce the switching frequency of the inverter and, thus, its losses which is in a 120 °C ambient temperature environment with only 55 °C margin to the upper junction temperature limit of Si power semiconductors a significant advantage.

3) Number of Phases: One-phase BLDC machines need less complex inverters than machines with a higher phase count. Either an H-bridge inverter with two high-side switches and

four switches in total supplying a single winding or two low-side switches supplying two separate windings connected in antiseries can be employed. This half-wave configuration needs only two switches, but the copper utilization is lower than for the H-bridge as each winding conducts only one half-wave. A significant drawback of one-phase machines is the asymmetry of the magnetic design needed to make sure that the machine can be put into rotation from any rotor position.

Two-phase BLDC machines having symmetric windings can be started from any rotor angle, but the drive inverter complexity is basically multiplied by two for the H-bridge or half-wave solution. It is also possible to use a single half-bridge for two windings if the midpoint of the series-connected windings is connected to the midpoint of supply. This solution though requires a supply voltage balancing and cuts the voltage that can be applied to the windings in half.

A three-phase BLDC machine appears as a reasonable compromise between the request for a symmetric machine design on the one hand and low drive effort on the other hand as the H-bridge of the one-phase machine needs to be extended by only one more bridge leg. Furthermore, a large variety of gate drivers for three-phase inverters and control ICs for three-phase BLDC machines is available as three-phase BLDC machines are widely used in industry. Hence, the BLDC machine for the high temperature fan will be designed as a three-phase machine.

III. Electrical Machine Design

A. Windings

The isolation of the windings has to withstand the sum of the maximum ambient temperature of 250 °C and the temperature rise due to ohmic losses in the windings as well as iron losses in the stator. High-temperature versions of conventional enameled copper wire can continuously withstand temperatures up to only 245 °C [38], [39]. A solution is copper wire, that is clad by nickel for increased oxidation resistance and coated by ceramic for electrical insulation. It can withstand temperatures up to 700 °C for more than 1′000 h and 425 °C for more than 5′000 h [40].

The resulting specific electrical resistance ρ_{CuNi} of the nickel clad copper wire can be calculated, if the fractions of nickel and copper cross sections are given. The "Kulgrid 28" wire used for this setup consists of $y_{\mathrm{Ni}} = 27\%$ nickel and $y_{\mathrm{Cu}} = 1 - y_{\mathrm{Ni}} = 73\%$ [41]. As the density of nickel is with 8.880 g/cm^3 less than 1% smaller than that of copper with 8.960 g/cm^3 at 20 °C [42], it is of negligible interest for the calculation of ρ_{CuNi} whether the volume or mass fractions are given. At higher temperatures, the densities match even better: Copper expands with $16.4 \times 10^{-6}1/\mathrm{K}$ and nickel with $13.1 \times 10^{-6}1/\mathrm{K}$ only.

If the wire cross-section is ideal such that a round copper conductor is encapsulated with a nickel clad of constant thickness, the following formula and results can be calculated from Ohm's law of parallel conductors using the specific electrical resistances $\rho_{\mathrm{Cu}} = 16.9\,n\Omega \cdot \mathrm{m}$ and $\rho_{\mathrm{Ni}} = 71.9\,n\Omega \cdot \mathrm{m}$ of copper and nickel, respectively, as well as their coefficients of the linear increase in resistivity with temperature, $\alpha_{\mathrm{Cu}} = 0.00391/\mathrm{K}$ and $\alpha_{\mathrm{Ni}} = 0.00661/\mathrm{K}$ [42],

$$\begin{aligned}\rho_{\mathrm{CuNi}} &= \frac{\rho_{\mathrm{Cu}} \cdot \rho_{\mathrm{Ni}}}{y_{\mathrm{Ni}} \cdot \rho_{\mathrm{Cu}} + y_{\mathrm{Cu}} \cdot \rho_{\mathrm{Ni}}} \\ &= \begin{cases} 1.26 \cdot \rho_{\mathrm{Cu}}(20\,^\circ\mathrm{C}) & \text{for} \quad T = 20\,^\circ\mathrm{C} \\ 1.29 \cdot \rho_{\mathrm{Cu}}(250\,^\circ\mathrm{C}) & \text{for} \quad T = 250\,^\circ\mathrm{C} \\ 2.44 \cdot \rho_{\mathrm{Cu}}(20\,^\circ\mathrm{C}) & \text{for} \quad T = 250\,^\circ\mathrm{C} \end{cases} \\ &= \begin{cases} 21.3\ \mathrm{n}\Omega \cdot \mathrm{m} & \text{for} \quad T = 20\,^\circ\mathrm{C} \\ 41.3\ \mathrm{n}\Omega \cdot \mathrm{m} & \text{for} \quad T = 250\,^\circ\mathrm{C}. \end{cases} \end{aligned} \tag{11}$$

(The conductivity of the wire is further affected by diffusion of nickel into the copper core. After 500 h of operation at 600 °C, the resistivity increases by another 25% for a wire with a fraction of 27% nickel [43].)

To avoid cracks of the ceramic insulation, the minimum bending radius of the ceramic coated nickel clad copper wire has to be at minimum ten-times larger than the outer diameter of the wire, which influences the design of the stator iron sheet package significantly (see Section III-B). For this setup, a wire with an external diameter of 0.1 mm is used.

The 30% increase of the winding resistance of the nickel clad copper wire compared to pure copper [see (11)], the expected lower fill factor (only 10% are assumed using the ceramic coated wire due to the mentioned mechanical properties limiting the winding area utilization) and the mentioned aim towards very small ohmic loses make the choice of a comparably low current density of in this case only 1 A/mm^2 necessary.

B. Stator Iron Sheet Package

The minimum bending radius of the ceramic coated wire (see Section III-A) means for the stator iron sheet package, that the tooth width has to be equal or larger than 2 mm. As higher numbers of teeth with a width of 2 mm would drastically reduce the winding area, the package is designed with six teeth (see Fig. 3). The number of poles is chosen to 8, as with a lower number, the yoke would increase in radial thickness and the winding factor of 0.87 for this combination is better or equally good than for 10 or more poles.

Eligible materials include iron with silicon (FeSi), nickel iron (NiFe), or iron cobalt (FeCo). FeSi is the cheapest material but has a lower saturation flux density and higher losses. Lowest losses and highest permeabilities offer NiFe. Highest flux density and, thus, highest torque and power density are possible with FeCo which makes it the favorable material for the high temperature fan.

"Vacoflux 48" by Vacuumschmelze shows a very narrow hysteresis loop ($H_{\mathrm{C}} < 40\,\frac{\mathrm{A}}{\mathrm{m}}$) and a high saturation flux density of $B_{\mathrm{S}} = 2.35$ T. The Curie temperature is $T_{\mathrm{C}} = 950\,^\circ\mathrm{C}$ and the coefficient of linear thermal expansion is $\alpha_{\mathrm{CTE}} = 9.5 \cdot \frac{10^{-6}}{\mathrm{K}}$. For this setup, 100 individual 0.1 mm thick sheets are used leading to an axial length of the machine of 10 mm. The sheets are laminated together for easier manufacturing. The adhesive used by Vacuumschmelze is only specified up to 190 °C, at higher temperatures it loses its adhesive effect and transforms into carbon which influences the behavior of the package: the temperature

of the material causes the hysteresis loop to shear so that the magnetic permeability decreases and the coercivity slightly increases. This leads to slightly higher losses (of about $+5\%$ for a temperature of 300 °C).

C. Permanent Magnets

The permanent magnets used in the high temperature fan need to have a sufficiently high remanence induction B_r and coercive force H_C at 250 °C. Hard magnetic materials with a high energetic product include neodymium iron boron (NdFeB) and samarium cobalt ($SmCo_5$ and Sm_2Co_{17}). For high temperature applications, the only possible material is SmCo. (Aluminum nickel cobalt (AlNiCo) is also possible, but has got a much lower energy product than SmCo.) Arnold Magnetics offers "Recoma" main grades as "Recoma HT" magnets, the latter for operating temperatures up to 520 °C. For the high temperature fan, "Recoma HT 420" magnets with a remanence of 0.9 T and an intrinsic coercive force of $1100\,\frac{\mathrm{kA}}{\mathrm{m}}$ at 250 °C are employed. The maximum demagnetization force applied to the magnets is $290\,\frac{\mathrm{kA}}{\mathrm{m}}$.

These magnets do not need to be protected against corrosion at 300 °C. At temperatures higher than 400 °C, they could be either packaged in a steel housing, which increases the length of the air gap of the machine, or coated with aluminum (up to 500 °C) or with nickel (up to 550 °C).

The magnet segments can be fit into the yoke and are fixed only by their magnetic force. Alternatively, they can be laminated into the yoke with adhesive based on silicon or ceramics. These adhesives though cannot absorb high thermo–mechanical stresses. The thickness of the magnets should not be lower than the actual 1 mm in order to make sure they do not break during manufacturing. If smaller thicknesses need to be realized, the magnets can be mounted into the yoke and then milled down to the desired thickness.

D. Yoke

The geometry of the yoke is chosen such that the flux density has a maximum value of 2 T. The air-gap is 0.3 mm. The material should have a relative permeability of 500 at this point for minimizing the reluctance of the magnetic path. Furthermore, the yoke's CTE should be close to that of the rotor as the yoke is directly fit into the rotor. The aforementioned cobalt iron alloy "Vacoflux 48" by Vacuumschmelze fulfills these criteria.

IV. Mechanics Design

In this section, the mechanical design of the high temperature fan, especially the choice of different technologies such as the bearing technology and the selection of the design concept as well as the materials are described, each with respect to the high temperature rating, the resulting thermal expansion and reduced strength of the materials and other constraints such as magnetic fields of the machine potentially causing eddy current losses.

The exploded view drawing in Fig. 4 shows the assembly of the individual fan components. The fan housing is the structural part of the fan. On the outlet side, there is a center borehole with inside thread. The bearing case is screwed into that hole. The plain bearings are shrunk into the bearing case and carry the shaft. The stator iron sheet package is shrunk onto the bearing case and ceramic coated copper windings are wound onto the stator. The permanent magnets of the electrical machine are mounted in the steel yoke which is then shrunk into the rotor. The rotor itself is shrunk onto the shaft at the fan inlet. The axial position of the rotor is determined by the magnetic force of the permanent magnets. Additionally, it can be fixed with respect to the plain bearing on the fan outlet using a small spring and a snap ring.

A. Shaft

The shaft is carried by plain bearings and, hence, it is very important that the thermal expansion of the shaft is close to that of the plain bearings, which is mainly determined by the bearing case (see Section IV-B). Otherwise for certain temperatures within the operating temperature range, either the bearing clearance has to be chosen very high resulting in high vibrations or the shaft gets stuck in the bearing.

In order to achieve a low coefficient of friction between the shaft and the bearing, the material is required to be harder than 40 HRC. Well suited material is steel (apart from chromium nickel steel and austenitic steel), e.g., chromium, nitrified or hard-chromium plated steel, or hard metal. Not suited is aluminum and its alloys or nonferrous metal. The roughness of the material should be lower than $1\,\mu$m for low friction. Reduction of the surface roughness can be achieved by surface finishing and polishing. The diameter of the shaft is determined by the mechanical load due to unbalance of the rotor, desired vibration reduction and mechanical resonance of the rotating shaft.

The shaft for this high temperature fan is made of a cylindrical pin, the material of this pin is steel 115CrV3 (also called steel 1.2210). It is hardened to 60 ± 2 HRC and its roughness class is N6, corresponding to a roughness depth of $R_\mathrm{a} < 0.8\,\mu$m. The coefficient of linear thermal expansion of the material is $13.7 \times 10^{-6} 1/\mathrm{K}$ for a temperature rise from 20 °C to 300 °C. The diameter of the pin is 3m6, i.e., 3 mm with a fit of m6 which is in absolute numbers $3\,\mathrm{mm}\,\binom{+0.008}{+0.002}$, and it is cut to a length 27.5 mm, i.e., the length of the shaft is reduced by 0.5 mm compared to the overall length of the fan in order to make sure that no rotating part overlaps the housing.

B. Bearing

5The choice of the bearing is crucial for the fan operation under high temperature conditions and is identified as the main impact factor on the lifetime of the fan. Generally, the bearings can be realized as:

1) roller bearing;
2) static or dynamic air bearing;
3) magnetically levitated bearing; or
4) plain bearing.

Magnetically levitated and air bearings are very complex, costly and not as compact as plain or roller bearings. Roller bearings need lubrication, and this is usually only used for temperatures below 200 °C. Some special greases are available up

to 260 °C and very rarely greases for higher temperatures are applicable.

The more cost effective and easier solution for the high temperature bearing is a plain bearing. Different materials are available for standard conditions, e.g., metal or solid polymer, mono-, bimetallic or sintered bearings, fiber-reinforced plastic composite, bronze or (artificial) carbon. Most materials are not applicable due to the high temperature the bearings are exposed to (the bearing losses make the bearing heat up to even higher temperatures), only bronze and carbon are suitable.

The carbon bearing is the only suited plain bearing for this purpose, if the high rim speed of the shaft is taken into account, which can be calculated as

$$v = \omega r = 2\pi \cdot 19\,000\,\mathrm{min}^{-1} \cdot 1.5\,\mathrm{mm} = 3.0\ \mathrm{m/s}. \qquad (12)$$

The dimensions of the bearing are determined by the requirements of the technology, i.e., the difference between the inner and outer radius is usually not less than 3 mm. For applications that have to be highly compact, the difference can be reduced to 2 mm because of the very small shaft diameter of 3 mm. This leads to an outer diameter of 7 mm and the axial length of the bearing is chosen to 4 mm.

The inner diameter of the bearing is given by the outer diameter of the shaft (3m6, i.e., 3 mm $\binom{+0.008}{+0.002}$, which will be reduced by approx. 6 μm by polishing the shaft). The inner diameter is furthermore influenced by the bearing clearance, that is given for dry operation from 0.3% to 0.5% of the shaft diameter. Lower clearances cause higher friction and thus higher losses and lower lifetime, higher clearance values cause higher vibrations. Also, the thermal expansion of the shaft (see Section IV-A) and the bearing has to be taken account when determining the inner bearing diameter. The bearing has a coefficient of linear thermal expansion of $5 \times 10^{-6} 1/\mathrm{K}$ which is comparably low, but is shrunk into the bearing case at a temperature that is 150 °C higher than the maximum operating temperature and, therefore, its thermal expansion is given by the bearing case (see Section IV-C).

C. Bearing Case

The material for the bearing case is required to have a CTE similar to the shaft, because the bearing expands just as its case does and similar to the CTE of the stator iron sheet package that is shrunk onto the casing in order to avoid high thermal stresses.

Furthermore, the material has to be nonmagnetic (i.e., should show a relative permeability $\mu_r \leq 1.0$, maintained also after cold working) in order to make sure that the time varying magnetic flux density in the stator is solely conducted by the stator iron sheet package and, hence, no eddy current losses in the bearing case occur.

The yield strength up to the maximum operating temperature has to be as high as possible because the carbon plain bearings are shrunk into the case. A high Young's Modulus makes sure, that the case even with a wall thickness of 0.5 mm at the inlet bearing is not widened excessively after shrinking in the bearings. This is important because the stator iron sheet package has to be shrunk onto the bearing case after mounting the bearings as the sheet package is not recommended to be exposed to higher temperatures than 400 °C which are necessary for shrinking in the bearing.

Titanium is available in many different alloys. The American organization ASTM International classifies 35 grades of different alloys. The most common grade is Titanium Grade 5 (also named by the material number 3.7164) which fulfills these requirements. Its coefficient of linear thermal expansion is $9.6 \times 10^{-6} 1/\mathrm{K}$.

The shape of the casing is defined by its function: it is screwed into the fan housing and, thus, needs a stopper to control the length of the screwing. The step on the outer diameter is needed to have a stopper for the stator iron sheet package when shrunk onto the case. The outer diameter is with 8 mm as small as possible; the difference between inner radius at the bearing collet and the outer radius of the case is only 0.5 mm. The length of the case is 24 mm, mainly given by the 28 mm overall length of the fan, again 0.5 mm clearance, and 3.5 mm for the shrink fit of rotor and shaft.

D. Rotor

The hub (24 mm outside) and blade (37 mm) diameter of the rotor as well as the blade shape are given by the fluid dynamic requirements (see Section II-D). The clearance between the rotor blades and fan housing is chosen to 0.5 mm due to manufacturing tolerances.

The material for the rotor must have high yield strength at high operating temperatures and a high resistance against fatigue cracks because of the high dynamic load caused by the rotations. The rotor is manufactured of Titanium Grade 5, just as the bearing case. The wall thickness is chosen to 0.5 mm as a tradeoff between electrical machine diameter that has to be maximized and mechanical strength at high temperatures. It can be seen from the FEM simulations in Fig. 5 that the areas of highest mechanical load are at the transitions between the inner cylinder and the blades. The maximum von Mises stress of 34 MPa at a rotational speed of 19 000 min^{-1} is more than a factor of 15 below the yield strength of Titanium Grade 5 at 300 °C. The maximum deformation is less than 6 μm at 19 000 min^{-1} at 300 °C and occurs at the blade tips.

E. Fan Housing

The stator guide vanes direct the air flow in a more axial direction to increase the efficiency of the heat sink. The material for the stator should have a CTE close to the CTE of the bearing case in order to have a similar thermal expansion when the bearing case is screwed into the housing and hence, the bearing case is also made of Titanium Grade 5. For easier manufacturing of the housing, it is produced in two parts: The first part containing the guide vanes shows an axial length of 7 mm, the second part contains the bore for the rotor. These two parts are laser beam welded, as can be seen in Fig. 1(b).

V. Experimental Results

To verify the previous theoretical considerations, experimental results are given in this section and summarized in Table I. The fan is driven by a commercial inverter "CC-75-400" employing sensorless control for high-speed permanent-magnet machines as manufactured by the company Celeroton [44]. The increased ambient temperature of up to 250 °C for the measurements is realized by a climate chamber "FD 53" by the company Binder [45]. All measurements are taken under stationary conditions, so that it is made sure that the temperature rise inside the fan due to its mechanical and electrical losses has reached is final value when measuring.

A. Fluid Dynamic Measurements

First, the fluid dynamic design target for the high temperature fan (similar characteristic at 120 °C as the Sanyo Denki reference fan at 20 °C) is validated on the fluid dynamic test bench of a large fan manufacturer. Fig. 5 shows the measured curve for 20 °C and 19 000 min^{-1}. To assess the design target, the curve for 120 °C and 19 000 min^{-1} as well as for the reference fan at 20 °C and 16′500 min^{-1} are also shown: The constraint given in (7) is fulfilled for the largest part of the operational curve the static pressure of the high temperature fan is significantly higher than for the reference fan with Δp_{HTF} dropping no more than 10% below Δp_{RF} very close to the region of stall.

It can also be seen, that the increased rotational speed does not only meet the requirements concerning Δp but also influences the volume flow according to (9). Measured $\dot{V}_{\max}$ is with $0.84\,\mathrm{m}^3/\mathrm{min}$ only 4.5% lower than calculated in (9).

B. Power Measurements

The considerations regarding the power rating of the fan are validated using a Yokogawa WT 3000 power analyzer [46]. Based on the data sheet value for the power of the reference fan (10.1 W) and (10), the high temperature fan is specified to 15 W (see Section II-D).

In the first power measurement, the input power of the reference fan is determined to 8.9 W with 12.0 V applied to its dc input (corresponding to its rated speed of 16′500 min^{-1}) at 25 °C and different operating points in its pressure versus volume flow curve (see Fig. 5). The difference of 12% to the power value given in the data sheet is caused by a safety margin of the specifications of the reference fan. This means according to (10), that the high temperature fan consumes 14.7 W at −40 °C and rated speed which is still below the design power consumption of 15 W. Hence, the fan can be operated at rated speed over the complete temperature range from −40 °C to 250 °C.

With this measurement, (10) can now be verified. The expected value for the power of the high temperature fan is 13.6 W, and the measured value is 11.5 W. The difference of 15% is due to the fact, that first the measured power for the high temperature fan does not include the power loss of the inverter driving the fan. Second, the design of the electrical machine for both fans varies significantly and a higher efficiency of the machine used for the high temperature fan compared to the reference fan can be assumed due to the use of magnets with a higher energy density and a three-phase design.

Measurements at higher temperatures proof (3): At 120 °C, a power consumption of 8.2 W is measured, which is 71% of the power measured at 20 °C (compared to 75% calculated). At 250 °C, 6.3 W are 55% of the power needed at 20 °C (compared to 56% calculated).

TABLE II
Weighted Total Sound Pressure Levels Measured at 25 °C

High Temperature Fan	66.6 dBA
Sanyo Denki San Ace 40 GV	65.0 dBA

C. Current and Voltage Waveforms

Figs. 6 and 7 show the phase voltages and currents, respectively, at 25 °C and at 250 °C under closed loop speed control. The 120 ° block shaped BLDC modulation scheme leads to clamped phase voltages during the short interval when all three phases conduct current due to nonzero phase inductance as can be seen from these figures. The amplitude of the phase voltages decreases slightly with temperature due to the decreasing remanence induction of the permanent magnets.

The current level is with an rms value of 0.8 A on the expected level, but shows a slight imbalance in phases A and C. This is due to small winding asymmetries leading to a slightly higher phase resistance in phase B. At high temperatures, the power level and, thus, the required torque and current decrease as has also been shown in Section V-B. Furthermore, it can be directly seen from the time base, that the period of a phase current is 0.79 ms leading to a rotational speed of 19 000 min^{-1} for this machine having four pole pairs.

D. Acoustic Measurements

As mentioned in Section II-A, the acoustic noise level of the high temperature fan is also of interest in this paper, especially as the rotational speed of the high temperature fan is increased by 15% compared to the commercial reference fan due to fluid dynamic requirements (see Section II-D).

The sound pressure level emitted by commercially available fans is usually measured according to the Japanese industry standard "JIS B 8330": A noise meter is placed in a distance of 1 m from the inlet side of the fan under test operated at its rated speed in an anechoic room [47]. Fig. 8 shows the sound pressure level over the audible frequency range measured at 25 °C for the high temperature fan and for the Sanyo Denki San Ace 40 GV fan. Due to the physical dimensions of the anechoic chamber used for this measurement, the microphone was placed in a distance of 0.2 m from the fan. To be able to compare the measurement result with the data sheet value of 58 dBA for the Sanyo Denki fan [28], the sound pressure level (declining with the inverse of the distance) has been scaled such as it would have been measured at 1 m distance.

Table II lists the total sound pressure levels for both fans which are calculated from Fig. 8 using a weighting of the different frequency components in order to take the properties of human

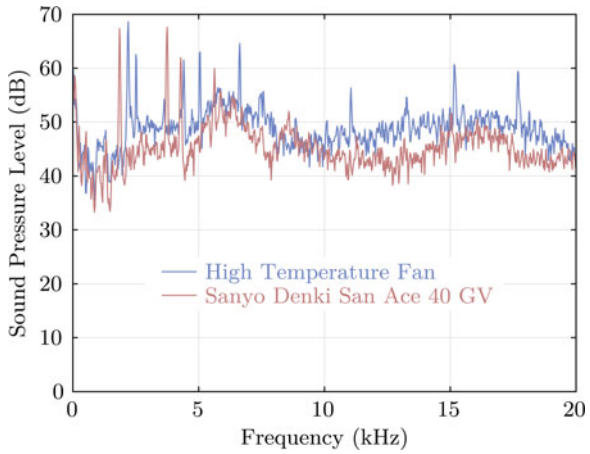

Fig. 8. Measured sound pressure level over the audible frequency range at 25 °C for the high temperature fan and the Sanyo Denki San Ace 40 GV fan (see Table II for calculated total sound pressure level).

hearing into account. The reason for the deviation is the air moving around the microphone in the test setup due to its small physical dimensions and the nonideality of the sound absorption at the chamber walls. The important result for this research is the difference in the weighted sound pressure level between the high temperature fan and the reference fan of only 1.6 dBA. This difference cannot be easily recognized by humans [48].

VI. Conclusion

In this paper, first the upcoming quest for 120 °C rated forced air-cooled power electronic converters in HEVs is motivated by showing the advantages of placing the converters as a part of the vehicles drive train underneath the engine hood. This creates the need for fans having a competitive fluid dynamic performance which are currently not commercially available at this temperature level. For certain cooling system setups in power electronic converters employing novel SiC semiconductors with elevated junction temperatures, these fans are required to operate up to 250 °C.

First, it was shown how the pressurization of the fan decreases at elevated temperatures and how the rotational speed can be increased to 19 000 min^{-1} to compensate this decline. Then, special focus was put on the design of the integrated BLDC machine for an ambient temperature of 250 °C, including magnetic material selection (Sm_2Co_{17} permanent magnets for the rotor and FeCo sheets for the stator package) and choice of ceramic coated CuNi windings introducing further constraints due to their minimum bending radius. The mechanical design of the fan for 250 °C operation and rim speeds up to $180\,\mathrm{m/min}$ with plain bearings is conducted. The selection of the materials for the different fan components has been done based on the evaluation of the material stresses, the material strength at 250 °C and the thermal expansion in an operating temperature range of almost 300 K, from −40 °C to 250 °C.

Finally, experimental results are given and are in good agreement with the theoretical considerations: the fluid dynamic characteristics, the power consumption, the voltage and current waveforms at room temperature, and an elevated temperature of 250 °C as well as the acoustic noise generation of the fan are measured.

References

[1] Z. Amjadi and S. S. Williamson, "Power-electronics-based solutions for plug-in hybrid electric vehicle energy storage and management systems," *IEEE Trans. Ind. Electron.*, vol. 57, no. 2, pp. 608–616, Feb. 2010.

[2] R. Schöttle and G. Threin, "Electrical power supply systems: Present and future," *VDI Berichte*, vol. 1547, pp. 449–475, 2000.

[3] FreedomCAR and Vehicle Technologies Program. (2007, Jun.). Plug-in hybrid electric vehicle R&D plan. U.S. Department of Energy, Working Draft. [Online]. Available: http://www1.eere.energy.gov/vehiclesandfuels/pdfs/program/phev_rd_plan_june_2007.pdf

[4] F. Renken and R. Knorr, "High temperature electronic for future hybrid powertrain application," presented at the Eur. Conf. Power Electron. Appl., Dresden, Germany, Sep. 11–14, 2005.

[5] S. Pischinger, M. Pischinger, H. Kemper, and S. Christiaens, "The challenges of system integration of the hybrid electric powertrain," presented at the Fachtagungsberichte VDE Kongress, Aachen, Germany, Oct. 23–25, 2006.

[6] J. Zhao and R. J. Seethaler, "A fully flexible valve actuation system for internal combustion engines," *IEEE/ASME Trans. Mechatronics*, vol. 16, no. 2, pp. 361–370, Apr. 2011.

[7] V. Pickert, H. Cheng, L. Pritchard, and D. J. Atkinson, "An experimental and computational study of water cooled heatsinks for HEV's," in *Proc. 5th IET Int. Conf. Power Electron., Mach. Drives*, Brighton, U.K., Apr. 19–21, 2010.

[8] J. B. Campbell, L. M. Tolbert, C. W. Ayers, B. Ozpineci, and K. T. Lowe, "Two-phase cooling method using the R134a refrigerant to cool power electronic devices," *IEEE Trans. Ind. Appl.*, vol. 43, no. 3, pp. 648–656, May/Jun. 2007.

[9] P. Godignon, X. Jorda, M. Vellvehi, X. Perpina, V. Banu, D. Lopez, J. Barbero, P. Brosselard, and S. Massetti, "SiC Schottky diodes for harsh environment space applications," *IEEE Trans. Ind. Electron.*, vol. 58, no. 7, pp. 2582–2590, Jul. 2011.

[10] J. M. Hornberger, E. Cilio, B. McPherson, R. M. Schupbach, A. B. Lostetter, and A. H. Mantooth, "A fully integrated 300 °C, 4 kW, 3-phase, SiC motor drive module," in *Proc. 38th IEEE Power Electron. Spec. Conf.*, Orlando, FL, USA, Jun. 17–21, 2007, pp. 1048–1053.

[11] P. Hagler, P. Henson, and R. Johnson, "Packaging technology for electronic applications in harsh high-temperature environments," *IEEE Trans. Ind. Electron.*, vol. 58, no. 7, pp. 2673–2682, Jul. 2011.

[12] T. J. Han, J. Nagashima, S. J. Kim, S. Kulkarni, and F. Barlow, "Implementation of a fully integrated 50 kW inverter using a SiC JFET based six-pack power module," in *Proc. IEEE Energy Convers. Congr. Expo.*, Phoenix, AZ, USA, Sep. 17–22, 2011, pp. 3144–3150.

[13] J. Biela, M. Schweizer, S. Waffler, and J. W. Kolar, "SiC versus Si — evaluation of potentials for performance improvement of inverter and dc-dc converter systems by SiC power semiconductors," *IEEE Trans. Ind. Electron.*, vol. 58, no. 7, pp. 2872–2882, Jul. 2011.

[14] M. Chinthavali, J. A. Tawfik, and R. V. Arimilli, "Design and analysis of a 55-kW air-cooled automotive traction drive inverter," in *Proc. 3rd IEEE Energy Convers. Congr. Expo.*, Phoenix, AZ, USA, Sep. 17–22, 2011, pp. 2345–2352.

[15] D. Bortis, B. Wrzecionko, and J. W. Kolar, "A 120 °C ambient temperature forced air-cooled normally-off SiC JFET automotive inverter system," in *Proc. 26th Ann. IEEE Appl. Power Electron. Conf. Expo.*, Ft. Worth, TX, USA, Mar. 6–10, 2011, pp. 1282–1289.

[16] R. Wang, P. Ning, D. Boroyevich, M. Danilovic, F. Wang, and R. Kaushik, "Design of high-temperature SiC three-phase ac-dc converter for 100 °C ambient temperature," in *Proc. 2nd IEEE Energy Convers. Congr. Expo.*, Atlanta, GA, USA, Sep. 12–16, 2010, pp. 1283–1289.

[17] B. Wrzecionko, J. Biela, and J. W. Kolar, "SiC power semiconductors in HEVs: Influence of junction temperature on power density, chip utilization and efficiency," in *Proc. 35th Ann. Conf. IEEE Ind. Electron. Soc.*, Porto, Portugal, Nov. 3–5, 2009, pp. 3834–3841.

[18] P. Ning, F. Wang, D. Jiang, D. Zhang, R. Lai, D. Boroyevich, K. Ngo, R. Burgos, K. Karimi, V. Immanuel, and E. Solodovnik, "Development of a 10-kW high temperature, high power density three-phase ac–dc–ac SiC converter," in *Proc. 3rd IEEE Energy Convers. Congr. Expo.*, Phoenix, AZ, USA, Sep. 17–22, 2011, pp. 2413–2420.

[19] (2010, Oct.). *Thermal Navigator*. HALA Contec GmbH & Co. KG, Ottobrunn, Germany. [Online]. Available: http://www.hala-tec.com/mod_use/dokumente/Thermal-Navigator_en.pdf
[20] *Cooling Systems—Technical Material*, Sanyo Denki Co., Ltd., Tokyo, Japan. [Online]. Available: http://db.sanyodenki.co.jp/product_db_e/coolingfan/pdf/e_spec.pdf
[21] *High Temperature Fans*, EVG Elektro-Vertriebs-Gesellschaft Martens GmbH & Co. KG, Mönchengladbach, Germany. [Online]. Available: http://www.evg.de/kataloge/En/EVG_1E10-english-022.pdf
[22] G. A. Landis, "Robotic exploration of the surface and atmosphere of Venus," *Acta Astronautica*, vol. 59, no. 7, pp. 570–579, 2006.
[23] A. König, "High temperature dc-to-dc converters for downhole applications," Ph.D. dissertation, Inst. Power Electron. Elect. Drives, RWTH Aachen Univ., Germany, Jun. 2009.
[24] Schlumberger Ltd. (2007). REDA hotline high temperature ESP systems. [Online]. Available: http://www.slb.com/~media/Files/artificial_lift/brochures/hotline_br.ashx
[25] B. Wrzecionko, A. Looser, J. W. Kolar, and M. Casey, "High-temperature (250 °C/500 °F) 19′000 rpm BLDC fan for forced air-cooling of advanced automotive power electronics," in *Proc. 37th Ann. Conf. IEEE Ind. Electron. Soc.*, Nov. 7–10, 2011, Melbourne, Australia, pp. 4162–4169.
[26] B. Wrzecionko, "High temperature / power density / output frequency SiC dc-ac converter system for hybrid electric vehicles," Ph.D. dissertation, Power Electron. Syst. Lab., ETH Zurich, Zurich, Switzerland, Sep. 2013.
[27] U. Drofenik, A. Stupar, and J. W. Kolar, "Analysis of theoretical limits of forced-air cooling using advanced composite materials with high thermal conductivities," *IEEE Trans. Compon., Packag. Manuf. Technol.*, vol. 1, no. 4, pp. 528–535, Apr. 2011.
[28] *San Ace 40 GV*, Sanyo Denki Co., Ltd., Tokyo, Japan. [Online]. Available: http://db.sanyodenki.co.jp/product_db/cooling/dcfan/group_pdf/1247013350.pdf
[29] G. Tan. (2008, Mar.). Fundamentals of brushless dc axial cooling fans. Sanyo Denki Co., Torrance, CA, USA, Tech. Rep., [Online]. Available: http://www.newark.com/pdfs/techarticles/sanyo/fundamentals_brushlessDCcoolingFans.pdf
[30] ebm Industries, Inc.. (1999). Motor design, quality and performance are critical to reliable operation of fans & blowers. ebm Industries, Inc., Werke, Germany, Tech. Rep., [Online]. Available: http://www.ebmpapst.us/pdfs/motor.pdf
[31] K. Stephan and P. Stephan, *Taschenbuch für den Maschinenbau*, 22nd ed. Berlin, Germany: Springer-Verlag, 2007, ch. D Thermodynamik, p. D 10.
[32] M. Hecht, T. Keilig, U. Kleemann, O. Polach, U. Seiffert, and R. Voit-Nitschmann, *Taschenbuch für den Maschinenbau*. 22nd ed., Berlin, Germany: Springer-Verlag, 2007, ch. Q Fahrzeugtechnik, p. Q 86.
[33] K. Stephan and P. Stephan, *Taschenbuch für den Maschinenbau*, 22nd ed. Berlin, Germany: Springer-Verlag, 2007, ch. D Thermodynamik, p. D 15.
[34] W. Wagner, *Lufttechnische Anlagen: Ventilatoren und Ventilatoranlagen*, 2nd ed. Würzburg, Germany: Vogel Buchverlag, 1997.
[35] P. L. Chapman and P. T. Krein, "Micromotor technology: Electric drive designer's perspective," in *Proc. 36th IEEE Ind. Appl. Conf.*, vol. 3, Chicago, IL, USA, 30 Sep.–4 Oct. 2001, pp. 1978–1983.
[36] C. Zwyssig, J. W. Kolar, and S. D. Round, "Megaspeed drive systems: Pushing beyond 1 million r/min," *IEEE/ASME Trans. Mechatronics*, vol. 14, no. 5, pp. 564–574, Oct. 2009.
[37] U. Kafader and J. Schulze, "Similarity relations in electromagnetic motors—limitations and consequences for the design of small dc motors," in *Proc. 9th Int. Conf. New Actuators (ACTUATOR)*, Bremen, Germany, Jun. 14–16, 2004, pp. 309–312.
[38] Elektrisola. (2011, Sep.). Enamelled copper wire acc to IEC—Europe. Elektrisola Dr. Gerd Schildbach GmbH & Co. KG., Reichshof-Eckenhagen, Germany. [Online]. Available: http://www.elektrisola.com/enamelled-wire/enamelled-wire-types/iec/europe.html
[39] Pack Feindrähte. (2011, Sep.). Technical data table for fine wires. Rudolf Pack GmbH & Co. KG., Gummersbach, Germany. [Online]. Available: http://www.pack-feindraehte.de/en/technical_data/fine_enamelled_copper_wires/magnet_wires.html
[40] Karl Schupp AG. Winding wires with ceramic insulation. Zollikerberg, Switzerland, Version 2.2. [Online]. Available: http://schupp.ch/gb/LTKR_ceramic_wires.htm
[41] Ceramawire High Temperature Magnet Wire Technical Specifications. Ceramawire, Elizabeth City, NC, USA. [Online]. Available: http://www.ceramawire.com/ceramaTechspec.pdf
[42] R. B. Ross, *Metallic Materials Specification Handbook*, 4th ed., London, U.K.: Chapman & Hall, 1992.
[43] J. R. Howell, "Composite wires for operation as electrical conductors at elevated temperatures," in *Proc. 7th Annu. Wire Cable Symp.*, Ashbury Park, NJ, USA, Dec. 2–4, 1958.
[44] (2012, Feb.). Celeroton Converter CC-75-400. Celeroton AG, Zurich, Switzerland. [Online]. Available: http://www.celeroton.com/datasheets/en/Datasheet-CC-75-400.pdf
[45] (2013, Jan.). Binder FD series 53 Drying ovens/Heating ovens, Binder GmbH, Tuttlingen, Germany.[Online]. Available: http://www.binder-world.com/mediadb/files/pdf/datenblatt-en/FD-53.pdf
[46] H. Iwase, O. Itou, and K. Tachibana. (2005). *WT3000 Precision Power Analyzer*, Yokogawa Electric Corporation, Tokyo, Japan. [Online]. Available: http://www.yokogawa.com/rd/pdf/TR/rd-tr-r00039-003.pdf
[47] Technical Material. Sanyo Denki Co., Ltd., Tokyo, Japan. [Online]. Available: db.sanyodenki.co.jp/product_db_e/coolingfan/pdf/technical_material.pdf
[48] G. Jones. (2011). Noise effects of cooling fans and its measurement. ebm-papst Automotive & Drives (U.K.) Ltd, Berkshire, U.K., Tech. Rep., [Online]. Available: http://www.ebmpapst-ad.com/media/content/technical_articles/TA_Noise-effects-of-cooling-fans-and-its-measurement.pdf

Benjamin Wrzecionko (S'08) received the Dipl.-Ing. degree from RWTH Aachen University, Aachen, Germany, in 2008, after his studies in electrical engineering at RWTH Aachen University and at the University of Bath, Bath, U.K. He received the Ph.D. degree from the Swiss Federal Institute of Technology Zurich (ETH Zurich), Zurich, Switzerland, in 2013, for his research on a high temperature / power density / output frequency SiC dc–ac converter system in the Power Electronic Systems Laboratory.

He is currently working on designated power electronic systems in the plant engineering and construction industry.

Andreas Looser (S'08) received the M.Sc. degree in electrical engineering from the Swiss Federal Institute of Technology (ETH) Zurich, Zurich, Switzerland, in 2007. He received the Ph.D. degree for his research on ultrahigh-speed electrical drive systems and bearing technology from the Power Electronic Systems Laboratory, ETH Zurich, in 2013.

Since 2013, he has been with Celeroton AG, Zurich, a spin-off company in the area of high-speed electrical drive systems. His research interests include mechatronics, power electronics, control, and microelectronics.

Johann W. Kolar (F'10) received the M.Sc. and Ph.D. degrees (*summa cum laude/promotio sub auspiciis praesidentis rei publicae*) from the University of Technology Vienna, Vienna, Austria.

Since 1984, he has been working as an Independent International Consultant in close collaboration with the University of Technology Vienna, in the fields of power electronics, industrial electronics, and high performance drives. He has proposed numerous novel converter topologies and modulation/control concepts, e.g., the VIENNA Rectifier, the Swiss Rectifier, and the three-phase ac–ac Sparse Matrix Converter. He has published over 400 scientific papers in international journals and conference proceedings and has filed more than 80 patents. He was appointed as a Professor and the Head of the Power Electronic Systems Laboratory at the Swiss Federal Institute of Technology (ETH) Zurich, Switzerland, on February 1, 2001. His current research interest includes ac–ac and ac–dc converter topologies with low effects on the mains, e.g., for data centers, more-electric-aircraft, and distributed renewable energy systems, and on solid-state transformers for smart microgrid systems. His further research interests include the realization of ultracompact and ultraefficient converter modules employing latest power semiconductor technology (SiC and GaN), micropower electronics and/or power supplies on chip, multidomain/scale modeling/simulation and multiobjective optimization, physical model-based lifetime prediction, pulsed power, and ultrahigh speed bearingless motors. He initiated and/or is the Founder/Cofounder of four spin-off companies targeting ultrahigh speed drives, multidomain/level simulation, ultracompact/efficient converter systems, and pulsed power/electronic energy processing. He is a Member of the Institute of Electrical Engineers of Japan (IEEJ) and of the International Steering Committees and Technical Program Committees of numerous international conferences in the field (e.g., Director of the Power Quality Branch of the International Conference on Power Conversion and Intelligent Motion). He is the founding Chairman of the IEEE PELS Austria and Switzerland Chapter and the Chairman of the Education Chapter of the EPE Association. From 1997 till 2000, he served as an Associate Editor of the IEEE TRANSACTIONS ON INDUSTRIAL ELECTRONICS and, since 2001, as an Associate Editor of the IEEE TRANSACTIONS ON POWER ELECTRONICS. Since 2002, he has also been an Associate Editor of the *Journal of Power Electronics* of the Korean Institute of Power Electronics and a Member of the Editorial Advisory Board of the *IEEJ Transactions on Electrical and Electronic Engineering*.

Dr. Kolar received the Best Transactions Paper Award of the IEEE Industrial Electronics Society in 2005, the Best Paper Award of the ICPE in 2007, the First Prize Paper Award of the IEEE IAS IPCC in 2008, the IEEE IECON Best Paper Award of the IES PETC in 2009, the IEEE PELS Transaction Prize Paper Award 2009, the Best Paper Award of the IEEE/ASME Transactions on Mechatronics 2010, the IEEE PELS Transactions Prize Paper Award 2010, the Best Paper First Prize Award at the ECCE Asia 2011, and the First Place IEEE IAS Society Prize Paper Award 2011. Furthermore, he received the ETH Zurich Golden Owl Award 2011 for excellent teaching. He also received an Erskine Fellowship from the University of Canterbury, Christchurch, New Zealand, in 2003. In 2006, the European Power Supplies Manufacturers Association (EPSMA) awarded the Power Electronics Systems Laboratory of ETH Zurich as the leading academic research institution in Power Electronics in Europe.

Michael Casey received the Engineering Science degree from Oxford University, Oxford, U.K. (first class honours), where he also received the D.Phil. degree for his thesis entitled "Cavitation inception on hydrofoils" in 1974.

He held postdoctoral positions at Durham and Cambridge Universities and then worked as an Engineer and Manager for nearly 30 years in various international companies (WS Atkins, Sulzer Turbo, Rolls Royce, and Sulzer Innotec), working on turbomachinery design, design methods, CFD, and experimental methods. From October 2003 to March 2011, he was Professor of Thermal Turbomachinery at Stuttgart University, Stuttgart, Germany. In retirement, he still acts as a Turbomachinery Consultant for PCA Engineers Limited in the U.K. and other organizations.

Dr. Casey is a Fellow of the Institution of Mechanical Engineers and of the American Society of Mechanical Engineers.